Optical Review (2023) 30:238–245
https://doi.org/10.1007/s10043-023-00793-0

SPECIAL SECTION: REGULAR PAPER

The 13th International Conference on Optics-Photonics Design & Fabrication (ODF'22), Sapporo, Japan

Si-microring resonator with sidewall nanograting structures for high-Q resonance modes

Anh Igarashi[1] · Koya Murooka[1] · Yasuo Ohtera[2] · Hirohito Yamada[1]

Received: 7 December 2022 / Accepted: 15 February 2023 / Published online: 13 March 2023

Abstract
A nanograting microring resonator is proposed for achieving concentric mode field profiles as the effect of guided-mode resonance. Based on a numerical simulation of the 2D finite-difference time-domain method, we clarified that the microring resonator with a combination of nanograting microring and sidewall blocks could generate two operating modes. The first is the optical whispering gallery mode, by which the light was in resonance inside the microring by total internal reflection and traveled in a circle around the microring. The second mode is guided-mode resonance, by which the light scattering from the grating structures is in resonance to create concentric magnetic-field distributions. The characteristics of resonance modes of the mode numbers, mode distribution, and Q factors are analyzed at the changes of the microring radius and the nanograting structures. A design of a nanograting bus waveguide with the same grating period as the nanograting microring is verified to achieve a high efficiency of the coupling ratio.

Keywords Nanograting · Resonance mode · Guided-mode resonance · Concentric field distribution

1 Introduction

Si-based microring resonator is one of the promising candidates for resonance cavities for all-in-one on-chip integrated photonic devices due to the advantages of simple structures and multiple narrow resonance peaks [1–4]. Microring resonator, which can support various resonances due to the light traveling in a circular cavity, has been studied in applications that need light generation in different wavelengths, such as optical filters and label-free biosensors [4–8]. For example, using a multi-radical microring design and side coupled to a signal waveguide, a microring resonator provides a narrow band and a large free spectral range dropping filter. Another example is in biosensing applications, in which the resonance wavelengths shift as a function of the refractive index of the attached biological analytes due to the interaction of the evanescence field and the biomolecules. Our research focuses on achieving high values of quality factors and mode distributions to employ multiple resonant modes.

There are two commonly discussed resonant modes in circular resonators: whispering gallery mode (WGM) and guided mode resonance (GMR). WGM resonator exhibits optical modes, in which the light is trapped in microcavities in total internal reflection (TIR) and travels in a circle without significant loss [9]. Several resonator structures are based on this principle, including microdisks, microrings, microbubbles, microspheres, etc. [10]. We focus on developing microring resonators due to the characteristics of easy fabrication on a planar substrate and large mode volume on the microring. Hence, the light travels inside the Si-microring waveguide and generates a resonant mode. On the other hand, the GMR effect is a resonance-coupled mode when an incident plane wave interacts with leaky waves generated by a high-index grating film [11–13]. It has been applied in designing filters and biosensors to achieve significant improvements [14, 15]. GMR effect is not only used in a flat surface but also could be observed by a cylindrical resonator with a

✉ Anh Igarashi
truong.hoang.anh.c6@tohoku.ac.jp

[1] Tohoku University, 6-6-05 Aramaki Aza Aoba, Aoba-ku, Sendai, Miyagi 980-8579, Japan

[2] Toyama Prefectural University, 5180 Kurokawa, Imizu, Toyama 939-0398, Japan

curved grating wall to achieve high Q factors at both low and high modes, enhancing mode volume in the circular cavity [16–18]. Much recent research focuses on mode control for more applications [19–22].

This paper proposes a Si nanograting microring resonator that can generate two types of WGM and GMR resonance modes by numerical calculation using finite-difference time-domain (FDTD) simulation. The resonator includes periodical-thinned waveguide-based microring and sidewall blocks. The light is confined by Fresnel reflection inside the waveguide as a conventional microring resonator, known as the effect of WGM. Another resonance mode comes from matching diffracted and reflected light caused by the grating structures. The guided light penetrates through the microring, and the leak light, which is from the nanograting structures generated as the GMR effect, forms concentric field profiles produced at the regions of the microring center. First, the resonance modes and the Q factors at high-order modes are demonstrated by optimizing the grating structures of the microring and sidewall blocks. Second, we propose a nanograting bus waveguide for coupling with the resonator, which can provide a high coupling ratio and retain intrinsic mode profiles. For further application, the research is driven by enhancing the field distribution based on the control of the resonance modes. The biosensing application is also discussed by controlling the quality factor at resonant mode. The proposed structures could improve the sensitivity for detecting the attached objects on the grating microring by enhancing the sensing surface [23]. Finally, we also discuss controlling the mode resonances for biosensing applications.

2 Structure and simulation method

A schematic of the proposed nanograting microring resonator is depicted in Fig. 1. A 220-nm-thick Si ($n_{Si} = 3.48$) nanograting microring is built on a SiO_2 substrate ($n_{SiO_2} = 1.44$), and an air layer ($n_{air} = 1$) as a cladding layer. The main grating microring, which is periodically side-thinned, has a waveguide width w of 500 nm, with a corrugation width Δw, and the grating length in the main microring a. Sidewall blocks, placed in the sides of the thinned grating microring, have a width (w_{side}) of 150 nm, a length of the sidewall blocks b, and a gap (g_{side}) of 50 nm. Grating period Λ is defined as the length from a grating structure of the main grating microring to the next sidewall block. The duty cycle of the grating (the ratio of the pillar and the grating period) is 0.8.

For the study of the resonance mode characteristics, the structure of the nanograting microring is simplified as a two-dimensional (2D) subject for the using 2.5D FDTD simulation (FullWAVE™ simulation tool; Synopsys), which requires less memory and calculation time, but which provides reliable results [18]. The effective refractive index of the nanograting structure microring was determined from a 3D-structured nanograting waveguide. The electromagnetic fields were uniform in the y direction normal to the paper plane. The calculation was considered in TM modes with H_y. The cavity was surrounded by an optimized perfectly matched layer to absorb the outgoing energy without producing reflections. In addition, the grid sizes were set with 0.01 μm grid size to obtain a tradeoff for accuracy and calculation time. Monitors of intensity calculations with FFT were placed at the microring resonator and the through port

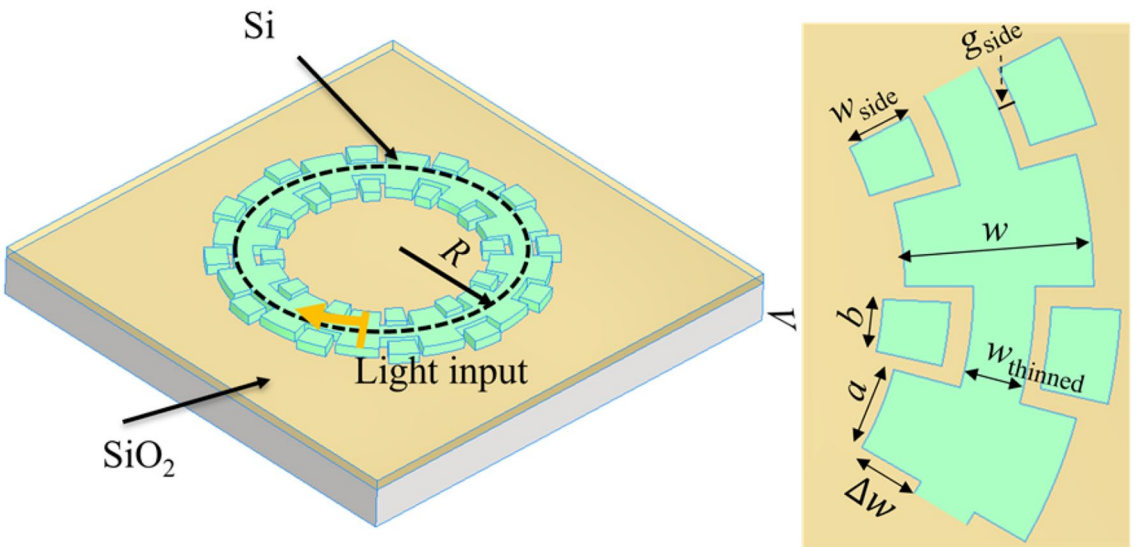

Fig. 1 Schematic of the nanograting microring resonator

of the bus waveguide to collect the transmission spectrum. The simulation time was set at 15 fs to obtain a wavelength resolution of 5 pm. A light source with impulse excitation was used to excite a wide range of frequencies in calculating the cavity resonances. Mode profiles were investigated using the excited light waves with resonance wavelengths.

In this research, the mode characteristics of intrinsic cavities of nanograting microring resonators were studied first to clarify the mechanism of the resonance modes. Features of the resonance modes are studied in Sect. 4, according to variation of center ring radius R, thinned width w_{thinned}, and the layout of grating structures. Later, a bus waveguide to couple the input light to the resonator would be optimized to obtain a low mode loss by side coupling.

3 Characteristics of resonance modes

Figure 2a presents the intensity spectrum of a nanograting microring resonator with R of 4.75 μm, Λ of 300 nm, w_{thinned} of 200 nm, $a = b = 240$ nm. An enlarged intensity spectrum from the wavelength of 1.3947 μm to 1.3955 μm are illustrated in Fig. 2b. The resonance wavelengths were noticed as the peak wavelength in the intensity spectrum. The resonance wavelength appears as the exact mechanism of a conventional microring resonator. When a light wave propagates through the resonator, the light energy inside the ring is built up when the resonance wavelength is satisfied

$$m\lambda = n_{eff} 2\pi R, \tag{1}$$

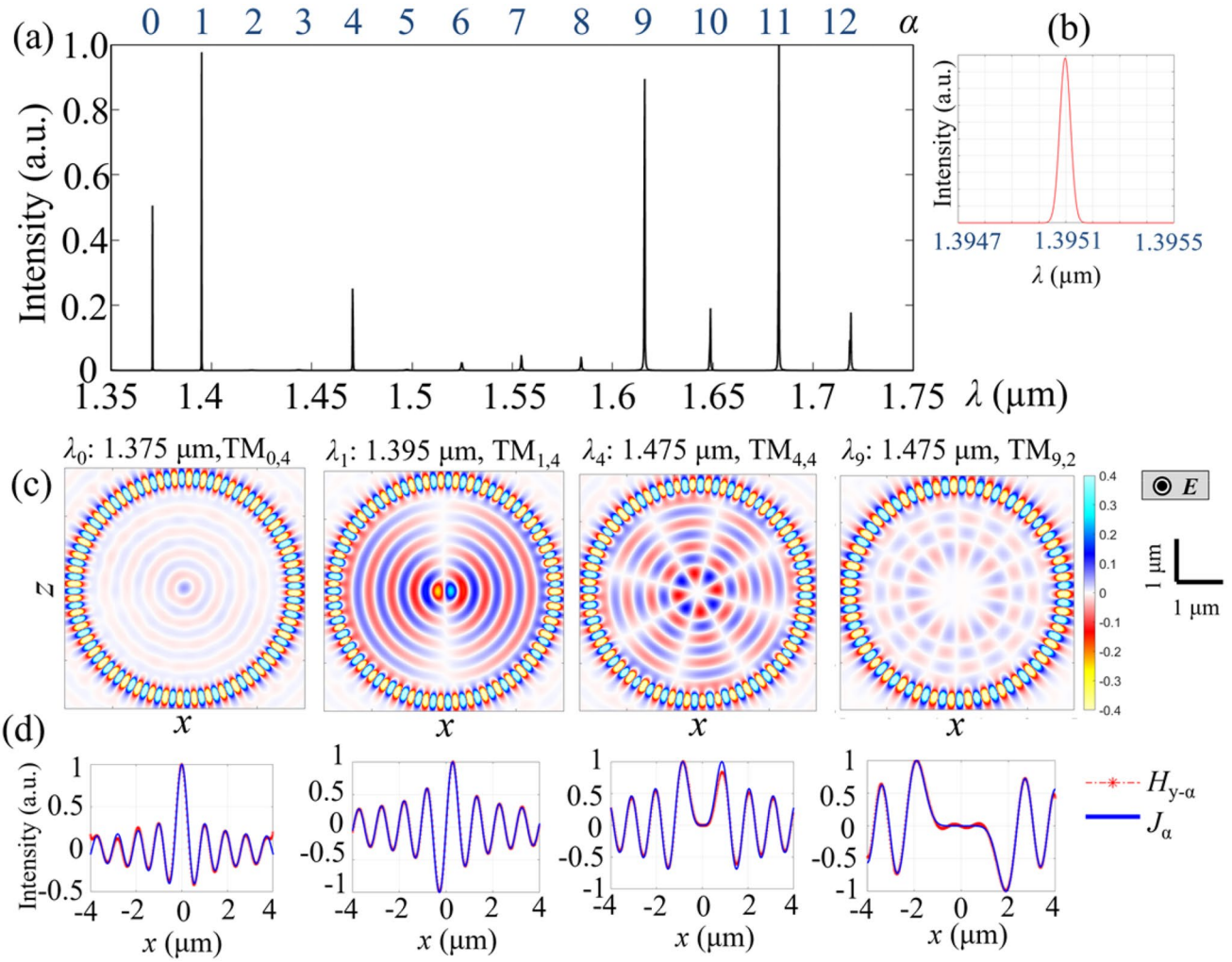

Fig. 2 Characteristics of nanograting microring resonator ($R = 4.75$ μm, $w_{\text{thinned}} = 200$ nm, $\Lambda = 300$ nm): **a** Intensity spectrum from $\lambda = 1.35$ μm to $\lambda = 1.75$ μm. Azimuthal mode numbers α are plotted on the upper side of the figure; **b** Enlarged view of intensity spectrum from $\lambda = 1.3947$ μm to $\lambda = 1.3955$ μm. **c** Resonance mode profiles at resonance wavelengths having azimuthal mode number of 0, 1, 4, 9; **d** Magnetic field distributions H_y and Bessel function along the x-axis when azimuthal mode number of 0, 1, 4, 9

where m is an integer, n_{eff} is the effective index of the nanograting microring, λ is the resonance wavelength, and R is the center radius. In this simulation, the material loss was not considered, so the system loss is the result of bending loss and propagating loss of the nanograting microring. Figure 2c shows the mode field profiles at different resonance wavelengths of 1.375 μm, 1.395 μm, 1.475 μm, and 1.615 μm. It is noteworthy that two patterns are formed along the azimuthal direction and radial direction. We designated the azimuthal mode number α as that along the azimuthal direction and radial mode number γ as that along the resonator radius. The azimuthal mode numbers α were plotted in Fig. 2a according to the increase of resonance wavelengths. The magnetic fields $H_{y-\alpha}$ at resonant modes α can be expressed under the α-th order of the Bessel function as

$$H_{y-\alpha} \propto J_{\alpha}\left(\frac{2\pi}{\lambda_{\alpha}} n_i r\right), \tag{2}$$

where λ_{α} is the wavelength of the incident light at the resonant mode α, n_{i} is the refractive index of the microring, and r is the radius. Figure 2d also indicates the cross-sections of magnetic intensity H_{y} (dotted red lines) and the Bessel functions for different mode numbers (solid blue lines). The magnetic fields inside the cavity were fitted with the Bessel functions at a low and high order of α. The values of γ are the numbers at which J_{α} becomes 0.

The Q factors at modes are calculated from the intensity spectrum by a function of $\lambda_{\alpha}/\lambda_{\alpha-FWHM}$, in which $\lambda_{\alpha-FWHM}$ is the wavelength difference of full width at half max. The Q factors at resonance with $\alpha = 0$, 1, 4, and 9 were, respectively, 2×10^5, 3.5×10^5, 5×10^4, and 1.5×10^5. The Q factor of a microring resonator (MRR) with a radius of 4.75 μm and width of 500 nm was around 9×10^3 under the same simulation conditions. Hence, the Q factors of nanograting microring resonators are 1–2 orders of magnitudes higher than the conventional microring resonator. The higher magnitude could be attributed to the GMR effect, by which the diffracted light from the leaked light from nanograting structures heads to the center of the microring, and the reflected light from the cavity center returns to the microring. Under several resonance wavelengths, when the reflected light and the propagated light waves are in the same phase, standing waves are formed as concentric light mode profiles, contributing a high Q factor.

4 Effect of nanograting structures on resonance modes

The microring radius, grating width, and sidewall blocks are the essential parameters to decide the matching of diffracted light from the grating structures and reflected light in the center microring and form the concentric resonance modes for higher-Q-factors at high mode orders. This part demonstrated the effect of ring radius, ring width, and side blocks.

Firstly, we compared the characteristics of the field modes and Q factors at different positions of the radius r in Eq. (2). The nanograting structures have the same parameters of Λ of 300 nm, w_{thinned} of 200 nm, $a = b = 240$ nm. Figure 3 is the 0-th order Bessel function J_0 along distance r (solid line), and the cross-section of magnetic field distribution H_{y-0} at the different center radius position (I), (II), and (III), which (I) is the radius of 3.46 μm, (II) is the radius of 3.68 μm, and (III) is the radius of 3.96 μm. The field mode profiles for these three different radii are the inset figures, depicted in the same figure. The resonance wavelength of this nanograting microring resonator is 1375.5 nm. Q factors in the cases of the center radius of 3.46 μm, 3.68 μm, and 3.96 μm are, respectively, 1.5×10^5, 7×10^3, and 1.8×10^5, respectively. When the center radius is 3.46 μm or 3.96 μm, where J_0 becomes valley or peak, the Q factors become high, and a stronger magnetic intensity exists inside the center ring. By contrast, when the center radius is 3.68 μm, by which J_0 becomes 0, the Q factor is low, and most of the resonance happens inside the waveguide by Fresnel reflection. As a result, the radius of nanograting microring could mostly decide the occurrence of the GMR effect.

In the next step, the resonance modes were evaluated by changing the microring grating width. The nanograting microring resonators have the same parameters of R of 4.75 μm, Λ of 300 nm, $a = b = 240$ nm, and different thinned widths w_{thinned} of 150 nm, 200 nm, 250 nm, and 300 nm. Figure 4 shows the Q factors according to the azimuthal modes α from 0 to 10, for different w_{thinned}. Accordingly, the ratio that the Q factors become the largest value for the same α is much

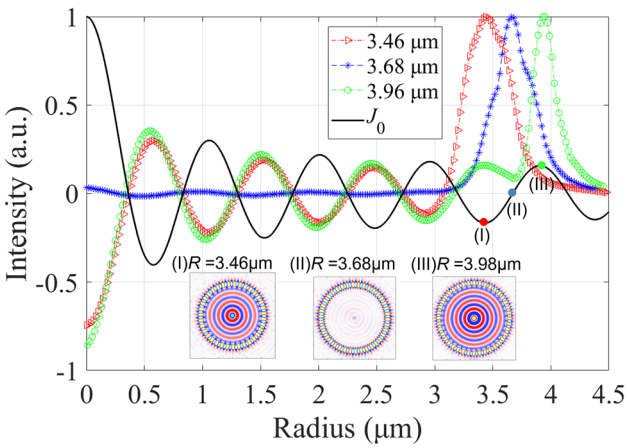

Fig. 3 H_{y} distributions at azimuthal mode number of 0 for different center radius position of (I), (II), and (III), which (I) is the radius of 3.46 μm, (II) is the radius of 3.68 μm, and (III) is the radius of 3.96 μm, and Bessel function (solid line) when the order α is 0. The inset figures are the resonance mode profiles at different radii of (I), (II), and (III)

the highest value of 5/11 when $w_{thinned}$ is 200 nm. When the thinned width was 300 nm, the Q factor was from 10^3 to 10^4, which is near to the Q factor of the conventional MRR, indicating that the strong resonance occurs in the waveguide as WGM resonance. The achieved highest Q factor of 3.5×10^5 occurred when $w_{thinned}$ is 200 nm at α of 1. The figure inset in Fig. 4 shows the shift of resonance wavelengths of different thinned widths according to the azimuthal mode numbers. As

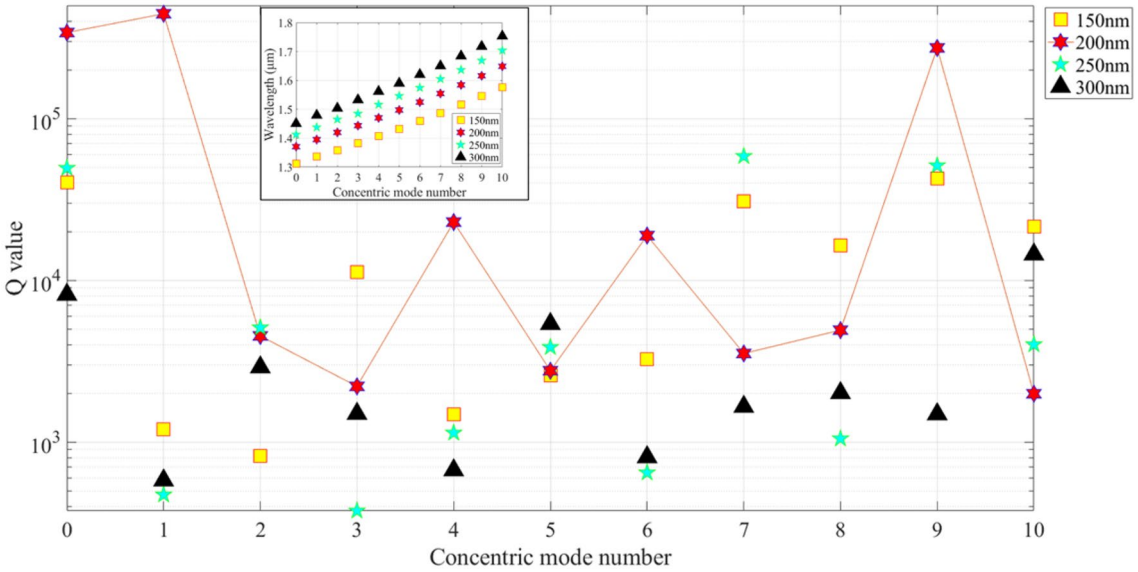

Fig. 4 Effect of waveguide widths on Q factor. The inset figure shows the resonance wavelengths along with the azimuthal mode numbers

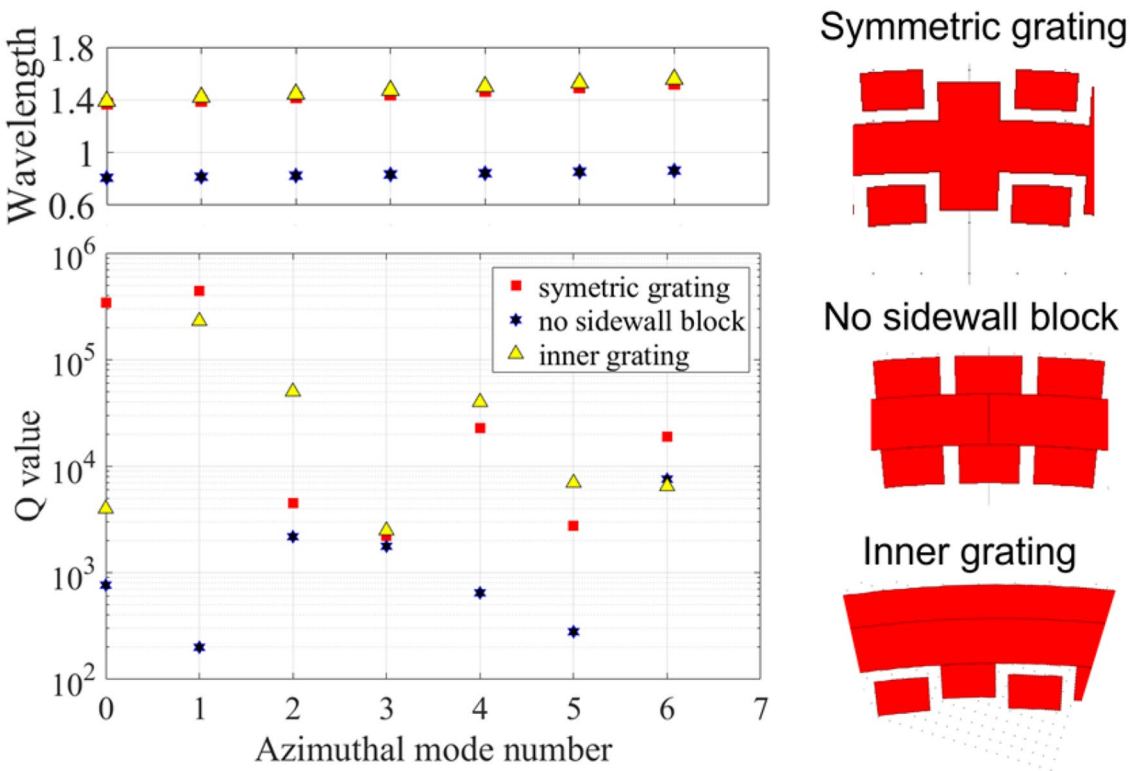

Fig. 5 Resonance wavelength shift and Q factors according to the azimuthal mode number with three nanograting structures: symmetric grating, no sidewall nanoblock, and inner grating

the width changes, the propagation constant changes for the light propagating inside microring and diffracted light from nanograting structures. Therefore, the resonance wavelengths will change together with the ring widths.

Finally, the resonance modes of nanograting resonators with the same Λ of 300 nm, but different nanoblock structures were evaluated. Three structures include a symmetric nanograting ring having sidewall nanoblocks (R of 4.75 μm), nanograting ring without sidewall nanoblocks (R of 4.75 μm), and inner nanograting having the sidewall nanoblocks on the interior side of microring (R of 4.82 μm). Figure 5 presents the wavelength shift with the azimuthal mode number and the Q factors at resonance wavelengths for three different nanoblock structures. Accordingly, the resonance wavelengths at $\alpha = 0$ of structures of the symmetric grating and the inner grating cavity are the same, while the wavelength resonance at $\alpha = 0$ of the no-sidewall-block shifted from 1.37 μm to 0.86 μm. This equality might be attributed to sidewall blocks, which support controlling the resonance wavelengths and more high-Q modes. The sidewall blocks affect the light direction and light intensity diffracted from the main waveguide to the concentric resonance. In addition, a high Q factor of 10^5 at $\alpha = 1$ was achieved when the value of R of the innergrating cavity was modified to 4.82 μm. Therefore, using the symmetric grating structure or inner grating cavity with sidewall blocks can obtain high Q factors at high modes.

5 Structures of bus waveguide for the coupling with the resonator

To generate the light penetrating to the nanograting microring resonator, we simulated transmission characteristics and mode profiles using two types of bus waveguides: a rectangular-type

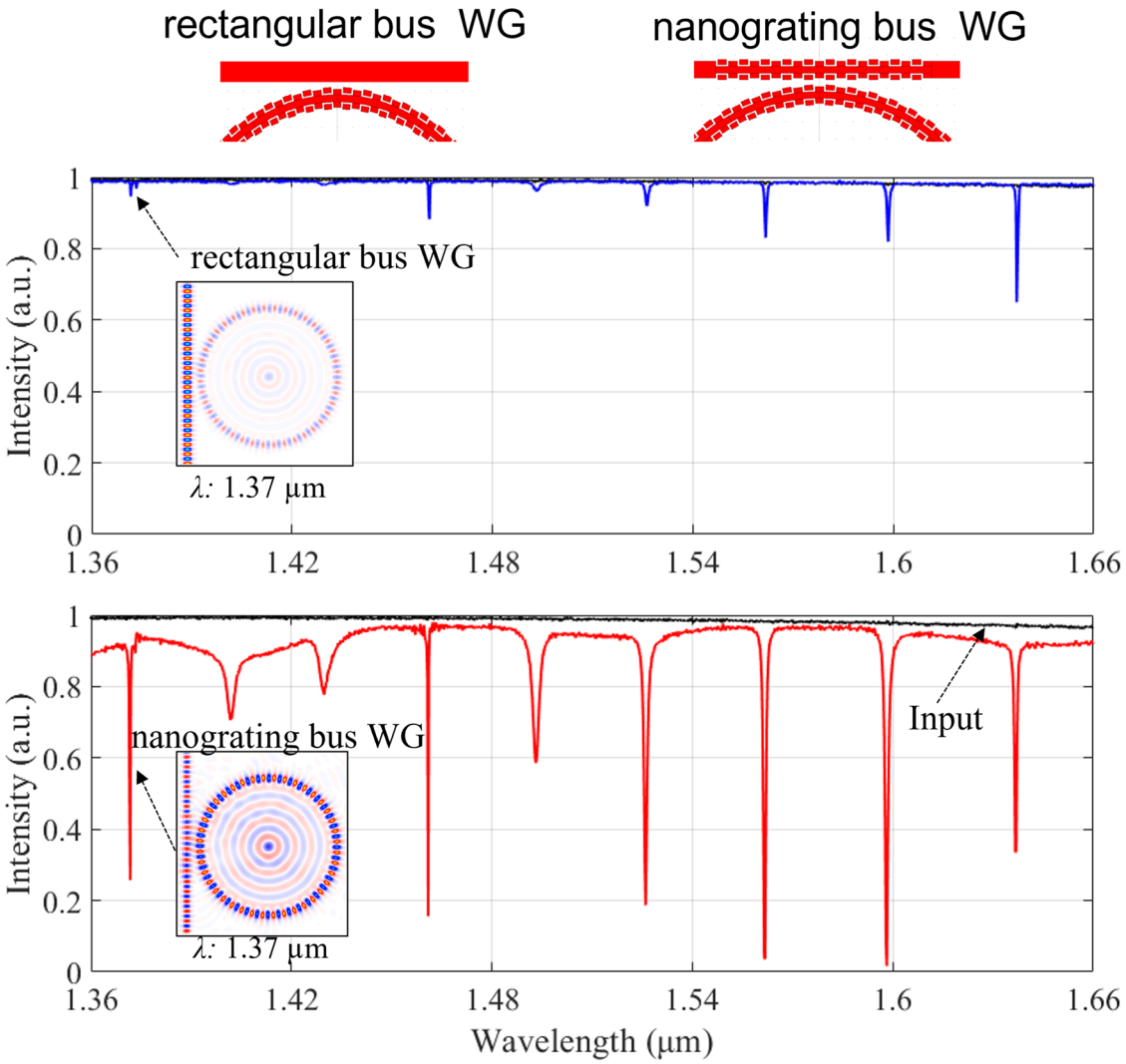

Fig. 6 Transmission spectrum of rectangular bus waveguide and nanograting bus waveguide

bus waveguide and a nanograting bus waveguide. The rectangular-type bus waveguide has a width of 500 nm, and the gap between the bus waveguide and the resonator was 200 nm. The nanograting bus waveguide has grating structures close to the resonator, which has a main width (w) of 500 nm, a w_{thinned} of 200 nm, a grating period of 300 nm, and 6 pairs of sidewall blocks. The nanograting microring resonator has a center radius of 3.96 μm. Power at the through port of the bus waveguide was monitored to obtain the spectral responses, as depicted in Fig. 6. The mode profiles at the azimuthal mode number of 0 are presented in the same figure.

The coupling ratio was calculated using the ratio of the optical power at the resonator and the input port. Results show that, at both structures of the bus waveguide, the input light was coupled with the resonator at the resonance wavelengths, which was the same value as the intrinsic resonator. However, the resonance using the nanograting bus waveguide is stronger than that of the rectangular bus waveguide. The coupling ratio of the rectangular waveguide and nanograting waveguide were 1.1% and 12%, respectively. In addition, whereas the Q factors at azimuthal mode number of 0 using rectangular was 6000, that of using the nanograting bus waveguide was 20,000. Therefore, a much stronger concentric resonance mode exists using the nanograting bus waveguide.

6 Application for biosensing using the change of mode characteristics

When the electromagnetic field exists in the central region of microring using the nanograting resonator, the transmission responses become sensitive to any attached substance on the resonator. The detection of a 1-μm-radius object in the central region of the resonator with a refractive index of 1.46 was simulated. Figure 7 indicates the mode profiles at the azimuthal mode number of 0, before and after the object had attached, using the nanograting microring resonator together with the nanograting bus waveguide ($R = 3.96$ μm). A stronger intensity of H_y was apparent after the object had attached. The Q factor changed from 1.9×10^4 to 6.7×10^3, and the wavelength shifted from 1373 to 1370 nm. These results indicate a sensing method for the attached object in the center ring of the nanograting microring resonator based on recognition of the change in mode characteristics of the Q factor and the wavelength shift.

7 Conclusions

We have presented simulation results of resonance modes of nanograting microring resonators. Light propagates through the microring as the effect of WGM resonance as conventional MRR. Because of the GMR effect for curved waveguides, the leaked light from the grating structures can formulate the concentric mode profiles. Structural parameter effects on the resonance mode exerted by the nanograting microring as ring radius, width, and sidewall blocks, on resonance mode were clarified. The Q factors and the concentric modes depend strongly on the position of the center radius of the microring. Furthermore, we designed nanograting bus waveguides that generated higher light coupling to the nanograting resonator than the conventional rectangular bus waveguide. Finally, we demonstrated a biosensing application using the change of Q-factor and resonance wavelength

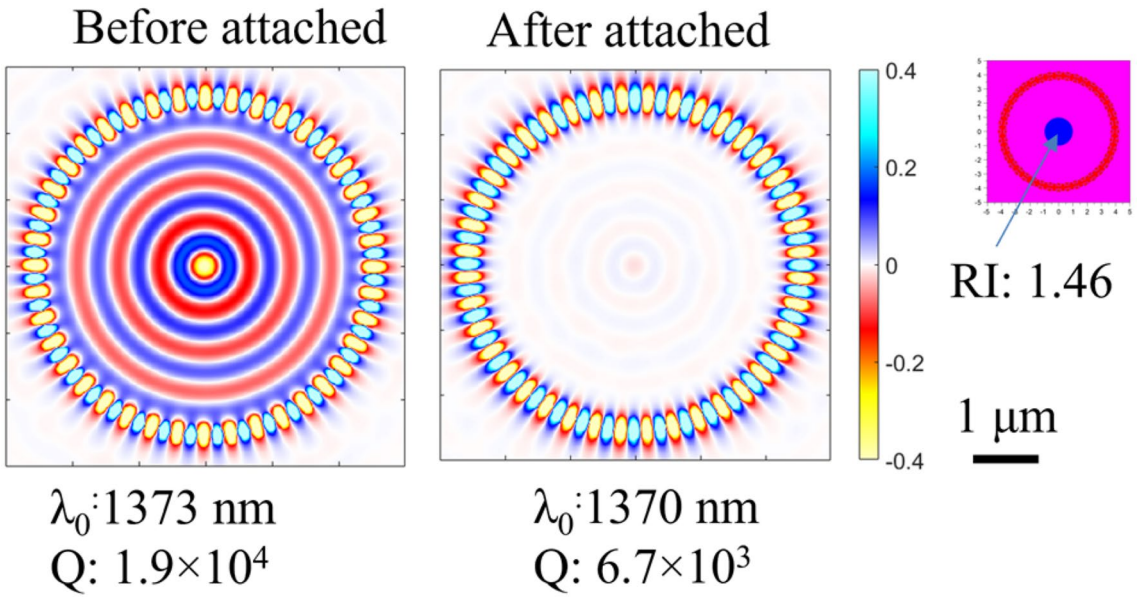

Fig. 7 Biosensing application uses the change of Q factor of nanograting microring resonator when an object attached is in the center ring

when the attached object is in the center ring of the resonator. Hence, the proposed nanograting structure would be a promising design for an ultra-sensitive microring resonator biosensor.

Acknowledgements This work was supported by JSPS Grant-in-Aid for Grant-in-Aid for Early-Career Scientists Numbers K22K145800 and by the Tohoku University Center for Gender Equality Promotion (TUMUG) Support Project.

Data Availability The data analyzed during the current study are confidential, but the authors will consider providing them upon reasonable request.

Declarations

Conflict of interest On behalf of all authors, the corresponding author states that there is no conflict of interest.

References

1. Schwelb, O.: Microring Resonator Based Photonic Circuits: Analysis and Design, 2007 8th International Conference on Telecommunications in Modern Satellite, Cable and Broadcasting Services, 187–194 (2007), doi: https://doi.org/10.1109/TELSKS.2007.4375971.
2. Park, T., Jeong, Y., Yu, K.: Cascaded optical resonator-based programmable photonic integrated circuits. Opt. Express **29**, 4645–4660 (2021)
3. Thirumaran, S., Dhanabalan, S.S., Sannasi, I.G.: Design and analysis of photonic crystal ring resonator based 6 × 6 wavelength router for photonic integrated circuits. IET Optoelectron. **15**, 40–47 (2021)
4. Xiao, S., Khan, M.H., Shen, H., Qi, M.: Compact silicon microring resonators with ultra-low propagation loss in the C band. Opt. Express **15**, 14467–14475 (2007)
5. Pasquazi, A., Ahmad, R., Rochette, M., Lamont, M., Little, B.E., Chu, S.T., Morandotti, R., Moss, D.J.: All-optical wavelength conversion in an integrated ring resonator. Opt. Express **18**, 3858–3863 (2010)
6. Vos, K.D., Bartolozzi, I., Schacht, E., Bienstman, P., Baets, R.: Silicon-on-Insulator microring resonator for sensitive and label-free biosensing. Opt. Express **15**, 7610–7615 (2007)
7. Steglich, P., Hülsemann, M., Dietzel, B., Mai, A.: Optical biosensors based on silicon-on-insulator ring resonators: a review. Molecules **24**(3), 519 (2019)
8. Flueckiger, J., Schmidt, S., Donzella, V., Sherwali, A., Ratner, D.M., Chrostowski, L., Cheung, K.C.: Sub-wavelength grating for enhanced ring resonator biosensor. Opt. Express **24**, 15672–15686 (2016)
9. Gugliandolo, G., Tabandeh, S., Rosso, L., Smorgon, D., Fernicola, V.: Whispering gallery mode resonators for precision temperature metrology applications. Sensors **21**, 2844 (2021)
10. Zhang, P., He, D., Zhang, C., Yan, Z.: FDTD simulation: simultaneous measurement of the refractive index and the pressure using microdisk resonator with two whispering gallery modes. Sensors **20**, 3955 (2020)
11. Wood, R.W.: On a remarkable case of uneven distribution of light in a diffraction grating spectrum. Proc. Phys. Soc. London **18**, 269 (1902)
12. Inoue, J., Ura, S., Kintaka, K.: Guided-mode resonance filter for micro-optic spectrometer," 2020 IEEE 70th electronic components and technology conference (ECTC), 1812–1817 (2020)
13. Wang, S.S., Magnusson, R.: Theory and applications of guided-mode resonance filters. Appl. Opt. **32**, 2606–2613 (1993)
14. Sahoo, P.K., Sarkar, S., Joseph, J.: High sensitivity guided-mode-resonance optical sensor employing phase detection. Sci. Rep. **7**, 7607 (2017)
15. Xiong, Y., Huang, Q., Canady, T.D., et al.: Photonic crystal enhanced fluorescence emission and blinking suppression for single quantum dot digital resolution biosensing. Nat. Commun. **13**, 4647 (2022)
16. Ohtera, Y., Iijima, S., Yamada, H.: Guided-mode resonance in curved grating structures. Opt. Lett. **36**, 1689–1691 (2011)
17. Ohtera, Y., Iijima, S., Yamada, H.: Cylindrical resonator utilizing a curved resonant grating as a cavity wall. Micromachines **3**, 101–113 (2012)
18. Ohtera, Y., Hirose, H., Yamada, H.: Characteristics of resonantly-guided modes in micro structured optical fibers. Photonics **1**, 432–441 (2014)
19. Jin, X., Yang, Y., Xiao, J., Huang, Y.: Mode control for microring resonators with inner-wall gratings. J. Opt. Soc. Am. B **33**, 1906–1912 (2016)
20. Petruškevičius, R., Balčytis, A., Urbonas, D., Vaškevičius, K., Juodkazis, S.: Microring resonators with circular element inner-wall gratings for enhanced sensing. J. Appl. Phys. **59**, SOOD02 (2020). https://doi.org/10.35848/1347-4065/ab9232
21. Wang, T., Zhang, Z., Liu, F., Tong, Y., Wang, J., Tian, Y., Qiu, M., Su, Y.: Modeling of quasi-grating sidewall corrugation in SOI microring add-drop filters. Opt. Commun. **282**(17), 3464–3467 (2009)
22. Yu, S.P., Lucas, E., Zhang, J., Papp, S.B.: A continuum of bright and dark-pulse states in a photonic-crystal resonator. Nat. Commun. **13**, 3134 (2022)
23. Truong, H.A., Shang, Y., Abe, S., Matsuda, N., Yamada, H.: Photonic biosensor for label-free detection based on photonic nanostructures on si-waveguide ring resonator. Eng Proc **6**(1), 39 (2021). https://doi.org/10.3390/I3S2021Dresden-10158